Opposing effects of reduced kidney mass on liver and skeletal muscle insulin sensitivity in obese mice

Chin, Siew Hung ; Item, Flurin ; Wueest, Stephan ; Zhou, Zhou ; Wiedemann, Michael S F ; Gai, Zhibo ; Schoenle, Eugen J ; Kullak-Ublick, Gerd A ; Al-Hasani, Hadi ; Konrad, Daniel

DOI: https://doi.org/10.2337/db14-0779

Opposing effects of reduced kidney mass on liver and skeletal muscle insulin sensitivity in obese mice

Siew Hung Chin[1,2,3], Flurin Item[1,2], Stephan Wueest[1,2], Zhou Zhou[4], Michael S. F. Wiedemann[1,2,3], Zhibo Gai[6], Eugen J. Schoenle[1,2], Gerd A. Kullak-Ublick[6], Hadi Al-Hasani[4,5], Daniel Konrad[1,2,3]

[1]Division of Pediatric Endocrinology and Diabetology and [2]Children's Research Centre, University Children's Hospital, CH-8032 Zurich, Switzerland

[3]Zurich Centre for Integrative Human Physiology, University of Zurich, CH-8057 Zurich, Switzerland

[4]German Diabetes Center at Heinrich Heine University and [5]German Center for Diabetes Research, D-40225 Düsseldorf, Germany

[6]Department of Clinical Pharmacology and Toxicology, University Hospital Zurich, CH-8091 Zurich, Switzerland

Correspondence to:

Daniel Konrad, MD PhD

University Children's Hospital

Department of Endocrinology and Diabetology

Steinwiesstrasse 75

CH-8032 Zurich

Tel: ++41-44-266 7966; Fax: ++41-44-266 7983

Email: daniel.konrad@kispi.uzh.ch

Diabetes Publish Ahead of Print, published online October 16, 2014

Abstract

Reduced kidney mass and/or function may result in multiple metabolic derangements, including insulin resistance. However, underlying mechanisms are poorly understood. Herein, we aimed to determine the impact of reduced kidney mass on glucose metabolism in lean and obese mice. To that end, seven-week-old C57BL6/J mice underwent uninephrectomy (UniNx) or sham operation. After surgery, animals were fed either a chow (standard) or a high fat diet (HFD) and glucose homeostasis was assessed 20 weeks after surgery. Intraperitoneal glucose tolerance was similar in sham-operated and UniNx mice. However, insulin-stimulated glucose disposal *in vivo* was significantly diminished in UniNx mice, whereas insulin-stimulated glucose uptake into isolated skeletal muscle was similar in sham-operated and UniNx mice. Of note, capillary density was significantly reduced in skeletal muscle of HFD-fed UniNx mice. In contrast, hepatic insulin sensitivity was improved in UniNx mice. Furthermore, adipose tissue HIF1α-expression and inflammation was reduced in HFD-fed UniNx mice. Treatment with the angiotensin II receptor blocker telmisartan improved glucose tolerance and hepatic insulin sensitivity in HFD-fed sham-operated but not UniNx mice. In conclusion, UniNx protects from obesity-induced adipose tissue inflammation and hepatic insulin resistance but it reduces muscle capillary density and, thus, deteriorates HFD-induced skeletal muscle glucose disposal.

Introduction

Metabolic disorders such as obesity, diabetes, and dyslipidemia may lead to progressive renal damage. Conversely, there is increasing evidence that reduced kidney function may deteriorate glucose metabolism and insulin sensitivity in humans (1; 2). In addition, live kidney donation may increase the risk to develop insulin resistance and the metabolic syndrome (3; 4). Such clinical observation is supported by recent experimental studies in rats showing the development of glucose intolerance, dyslipidemia, and ectopic fat accumulation in parallel with the development of uremia in uninephrectomized animals (5; 6). Mechanistically, overnutrition may activate the renin angiotensin system (RAS) and, thus, may contribute to the pathogenesis of the metabolic syndrome in the presence of reduced renal function. In particular, activation of the RAS/angiotensin receptors (ATRs) impairs insulin signaling in adipose tissue, skeletal muscle and liver (7) and its prevention by ATR blockade (pharmaceutically or genetically) improves glucose homeostasis (8; 9). In particular, the angiotensin II type 1 receptor blocker telmisartan was previously reported to improve obesity-/HFD-associated adipose tissue inflammation (10-12). Moreover, uninephrectomized rats developed fat redistribution that could be prevented by treatment with an angiotensin-converting enzyme (ACE)-inhibitor (6).

Skeletal muscle is the major site of insulin-induced glucose disposal in the postprandial state. Besides directly stimulating glucose uptake into muscle fibers, insulin increases microvascular blood flow to the muscle accounting for approximately half of the insulin-mediated glucose uptake (13). Accordingly, the number of capillaries perfusing the muscle is positively related to peripheral insulin action (14). Moreover, reduced blood flow to the muscle is correlated with insulin resistance (15-18) and

insulin-resistant humans and rodents exhibit capillary rarefaction (19-21). However, it still remains unclear whether the reduction in capillaries is a cause or consequence of muscle insulin resistance (22).

In the present study, we sought to determine the impact of reduced kidney mass as established by uninephrectomy (UniNx) on glucose metabolism in HFD-fed mice. Unexpectedly, we found that UniNx resulted in decreased adipose tissue inflammation and improved hepatic insulin sensitivity and steatosis. In contrast, UniNx reduced skeletal muscle capillary density and deteriorated muscle insulin action *in vivo*.

Research Design and Methods

Animals

Male C57BL/6J (C57BL/6JOlaHsd)-mice were purchased from Harlan (AD Horst, The Netherlands). All mice were housed in a specific pathogen-free environment on a 12-hourlight-dark cycle (light on from 7 pm to 7 am) and fed *ad libitum* with regular chow diet (ProvimiKliba, Kaiseraugst, Switzerland) or high fat diet (HFD) (58 kcal% fat w/sucrose Surwit Diet, D12331, Research Diets). All protocols conformed to the Swiss animal protection laws and were approved by the Cantonal Veterinary Office in Zurich, Switzerland.

Surgical procedures

Male C57BL/6J mice underwent uninephrectomy or sham operation at seven weeks of age. Mice were anesthetized with isoflurane (Abbott, Baar, Switzerland). Mice were placed on a warming-pad and kept under an infrared heating lamp to stabilize body temperature during the whole surgical procedure. Left nephrectomy was performed through a 1.0 cm incision on left dorsolateral paralumbar region as follows. After skin incision, abdominal muscles were incised to expose retroperitoneal region. Left kidney was secured with a clamp (FRANCIS chalazion forceps, D-8425) and fat attached to kidney was removed. Special care was taken to prevent damage to the adrenal gland. Renal blood vessels and ureter were ligated with sterile silk surgical sutures. Subsequently, left kidney was excised distal to ligatures. Abdominal muscles were sewn with reabsorbal thread and opposite ends of incised skin was clipped together using sterile disposable skin staplers. Sham-operated control mice underwent identical

surgical procedure except for kidney removal. Subcutaneous injection of buprenorphine (Essex, Luzern, Switzerland) every 6 hours for 2 days was used for analgesia.

Intra-peritoneal glucose and insulin tolerance tests

For intraperitoneal glucose tolerance test (ipGTT) mice were fasted overnight and for intraperitoneal insulin tolerance tests (ipITT) for 3h. Either glucose (2 g/kg body weight) or human recombinant insulin (1.0 U/kg body weight) were injected intraperitoneally (23).

Glucose clamp studies

Glucose clamp studies were performed as described (24). Clamps were performed in freely moving mice. Glucose infusion rate was calculated once glucose infusion reached a more or less constant rate with blood glucose levels at 5 mmol/l (80–90 min after the start of insulin infusion). Thereafter, blood glucose was kept constant at 5 mmol/l for 20 min and glucose infusion rate was calculated. The glucose disposal rate was calculated by dividing the rate of [3-^{3}H]glucose infusion by the plasma [3-^{3}H]glucose specific activity (25). Endogenous glucose production during the clamp was calculated by subtracting the glucose infusion rate from the glucose disposal rate (25; 26). Insulin-stimulated glucose disposal rate was calculated by subtracting basal endogenous glucose production (equal to basal glucose disposal rate) from glucose disposal rate during the clamp (27). In order to assess tissue specific glucose uptake, a bolus (10 µCi) of 2-[1-^{14}C]deoxyglucose was administered via catheter at the end of the steady state period. Blood was sampled 2, 15, 25 and 35 min after bolus delivery. Area under the curve of disappearing plasma 2-[1-^{14}C]deoxyglucose was used together with tissue-

concentration of phosphorylated 2-[1-^{14}C]deoxyglucose to calculate glucose uptake, as was previously described (28).

Metabolic cage analysis

Locomotion, food intake, O_2 consumption and CO_2 production were determined for single housed mice during a 24-h period in a metabolic and behavioral monitoring system (PhenoMaster, TSE Systems, Bad Homburg, Germany) as described (29).

Determination of insulin, free fatty acid, angiotensin I, creatinine, uric acid and bile acid levels

Plasma insulin and free fatty acid levels were determined as described (23). Plasma angiotensin I levels were determined by an ELISA kit (Cusabio Biotech CO Ltd, Wuhan, PR China). Serum creatinine levels were measured using DetectX® Low Sample Volume Serum Creatinine Kit (K0021-H1D, Arbor Assays, Ann Arbor, MI, USA), serum uric acid levels by QuantiChrom™ Uric Acid Assay Kit (DIUA-250, BioAssay Systems, Hayward, CA, USA) and plasma bile acid levels using Mouse Total Bile Acids Assay Kit (80470, Crystal Chem Inc, Downers Grove, IL, USA).

Glucose incorporation into isolated soleus and EDL muscle

Mice were fasted for 4 h prior to the analysis. EDL and soleus muscles were removed from anesthetized mice (Avertin, 99% 2,2,2-tribromo ethanol, and tertiary amyl alcohol at 15–17 µl/g body weight ip) and incubated for 30 min at 30°C in vials containing preoxygenated (95% O_2-5% CO_2) Krebs-Henseleit buffer (KHB) containing 5 mM HEPES (prebuffer) and supplemented with 15 mM mannitol and 5 mM glucose.

Muscles were transferred to new vials containing fresh pre-gassed KHB, as described above with or without 120nM of insulin (Actrapid; Novo Nordisk, Mainz, HE, Germany). Afterwards, muscles were transferred to new vials containing preoxygenized KHB supplemented with 20 mM mannitol and incubated for 10 min. Muscles were then transferred to new vials containing preoxygenized KHB supplemented with 1 mM [^{3}H]2-deoxy-glucose (2.5 µCi/ml), and 19mM [^{14}C]mannitol to account for extracellular space, and incubated for 20 min. After the last incubation, muscles were washed in ice-cold KHB, dried externally on filter paper, and quickly frozen with aluminum tongs precooled in liquid nitrogen and stored at −80°C. Glucose transport rates were determined by scintillation counting of cleared protein lysates as described (30).

Insulin signaling in skeletal muscle ex vivo

For assessing insulin-stimulated Akt phosphorylation in skeletal muscle, insulin (2U/kg) was injected i.p. in mice fasted for 5 hours. Skeletal muscles (quadriceps) were harvested 15 minutes after insulin injection, snap frozen in liquid nitrogen and stored at -80°C until homogenization.

Histology

Fat tissues were fixed in 4% buffered formalin and embedded in paraffin. Sections were cut and stained with hematoxylin and eosin. For each fat pad at least 100 adipocytes were analyzed. Quadriceps femoris muscle was mounted in embedding medium (o.c.t. embedding matrix, CellPath Ltd., Newtown, UK), snap frozen in isopentane cooled to -160°C with liquid nitrogen, and subsequently stored at -80°C until use. Consecutive 12 µm sections were cut on a microtome at -25°C. Rat anti-mouse

CD31 endothelial cell antibody (BioLegend, San Diego, CA) was used as a marker for muscle capillaries, and capillary-to-fiber ratio was calculated by dividing the number of CD31-positive cells by the number of muscle fibers. For all histochemical and immunohistochemical analyses NIH Image J software (National Institutes of Health, Bethesda, MD) was used.

Total liver lipid and triglyceride determination

Liver tissue (10-30mg) was homogenized in PBS and lipids were extracted in a chloroform-methanol (2:1) mixture. Total liver lipids were determined by a sulfophosphovanillin reaction as previously described (31). Liver triglycerides were measured from 50 mg of liver tissue using a variation of the Bligh and Dyer method (32) and quantified with an enzymatic assay (Roche Diagnostics, Rotkreuz, Switzerland).

RNA extraction and quantitative reverse transcription-PCR (RT-PCR).

Total RNA was extracted and reverse transcribed as described (33). The following primers were used: TNF-α Mm00443258_m1, IL-6 Mm00446190_m1, IL-1β Mm0043422/8_m1, cd11c Mm00498698_m1, ATGL Mm00503040_m1, perilipin Mm00558672_m1, HIF1α Mm00468869_m1, CD31 Mm01242584_m1, VEGF-A Mm01281441_m1 (Applied Biosystems, Rotkreuz, Switzerland).

Western Blotting

Cells or tissues were lysed and Western blots were performed as previously described (33). The following primary antibodies were used: anti-phospho-Akt (Ser473),

anti-total Akt (Cell Signaling, Danvers, MA, USA), anti-VEGF-A (Santa Cruz Biotechnology Inc., Dallas, TX, USA) and anti-actin (Millipore, Zug, Switzerland).

Data analysis

Data are presented as mean +/- SEM and were analyzed by unpaired Student's *t* test. p-Values < 0.05 were considered significant.

Results

Improved hepatic but deteriorated muscle insulin sensitivity in HFD-fed UniNx mice

Surgical procedure (sham operation or UniNx) was performed in C57BL6/J mice at seven weeks of age. Mice were fed either normal chow or HFD for 20 weeks. Total body weight gain was similar in sham-operated and UniNx mice under both diets (Table 1). After 20 weeks of HFD, inguinal and mesenteric fat pad weights in the UniNx mice were comparable to sham-operated mice, whereas epididymal fat pad weight was significantly higher in UniNx mice (Table 1). No differences in fat pad weights were observed between chow-fed sham-operated and UniNx mice (Table 1). In addition, food intake, locomotion, or fuel utilization (respiratory quotient, RQ) was similar between HFD-fed sham-operated and UniNx mice (Supplementary Figure 1).

Fasting blood glucose levels were similar between HFD-fed sham-operated and UniNx mice (Table 2). In addition, plasma insulin and free fatty acid (FFA) concentrations did not differ significantly between both groups (Table 2). Glucose and insulin tolerance were similar in UniNx mice compared to sham-operated mice under both standard chow as well as HFD 20 weeks after surgery (Figures 1A and 1B). Hyperinsulinemic-euglycemic clamp studies revealed similar glucose infusion rate in HFD-fed UniNx compared to sham-operated mice (see Figure 1C for steady-state glucose infusion rates and Supplementary Figure 2 for detailed time courses). Importantly, insulin-induced suppression of endogenous glucose production (mainly reflecting hepatic glucose production) was blunted in HFD-fed sham-operated mice, but was clearly evident in UniNx mice (Figure 1D) indicating improved/preserved hepatic insulin sensitivity in the latter. In contrast, glucose disposal rate during hyperinsulinemic-

euglycemic clamp was significantly further deteriorated in HFD-fed UniNx mice suggesting reduced skeletal muscle insulin sensitivity compared to sham-operated mice (Figure 1E).

Improved hepatic steatosis in HFD-fed UniNx mice

Hepatic insulin sensitivity is often associated with hepatic steatosis, though it is still debated whether insulin resistance is the cause of hepatic steatosis, or whether the increase in triglycerides (or of lipid metabolites such as ceramides, diacylglycerol and acyl-CoAs) causes the development of hepatic and/or systemic insulin resistance. As depicted in Figure 2A, total liver lipid content was greatly reduced in HFD-fed UniNx compared to sham-operated mice. Similarly, liver triglyceride levels were reduced in HFD-fed UniNx mice (UniNx mice: 234.5 ± 41.0 µmol/g liver; sham-operated mice: 401.3 ± 77.5 µmol/g liver). In addition, histological examination of liver sections revealed reduced frequency of lipid vacuoles in HFD-fed UniNx mice (Figure 2B).

Reduced adipose tissue inflammation in HFD-fed UniNx mice

The ‘portal theory’ proposes that the direct exposure of the liver to increasing amounts of FFA and/or pro-inflammatory factors released from visceral fat into the portal vein may promote the development of hepatic insulin resistance and steatosis (34). Accordingly, mRNA expression of pro-inflammatory cytokines as well as adipose tissue histology was analyzed in order to characterize adipose tissue inflammation. As depicted in Figure 2C, expression of CD11c (a marker for pro-inflammatory M1 polarized macrophages) and interleukin-6 (IL-6) was significantly decreased and expression of tumor-necrosis factor alpha (TNFα) and interleukin-1 beta (IL-1β) trendwise reduced in

mesenteric adipose tissue of HFD-fed UniNx compared to sham-operated mice. Of note, mRNA levels of the hypoxia-inducible factor 1α (HIF1α) was significantly lower in mesenteric adipose tissue of HFD-fed UniNx mice (Figure 2C). In contrast, adipocyte size was not different between both groups of mice (Figures 2D and 2E). In addition, insulin-stimulated Akt-phosphorylation in adipose tissue was similar in both groups suggesting similar insulin sensitivity in this tissue (Figure 2F). Thus, uninephrectomy protects mice from the development of HFD-induced adipose tissue inflammation and consequently hepatic insulin resistance.

Similar skeletal muscle insulin action in vitro

Glucose uptake into isolated soleus (slow-twitch) and extensor digitorum longus (fast-twitch) muscles was assessed next removing extramyocellular barriers to muscle glucose uptake. As depicted in Figure 3A and B, basal and insulin-stimulated glucose uptake were similar between HFD-fed sham-operated and UniNx mice, suggesting no direct impairment of insulin action at the myocyte level. Of note, 20 weeks of HFD led to an expected poor insulin response in skeletal muscle, which was particularly evident in soleus muscle. Similar to *ex vivo* glucose uptake, no difference between both groups of mice was found for *in vivo* insulin-stimulated Akt phosphorylation in total muscle homogenates (Figure 3C). These data in isolated muscle contrasts the data obtained from hyperinsulinemic-euglycemic clamp studies revealing diminished muscle insulin sensitivity in HFD-fed UniNx mice and may indicate that UniNx leads to impaired insulin delivery to the sarcolemma, e.g. through reduction in capillary density.

Reduced capillary density in skeletal muscle of HFD-fed UniNx mice

In order to assess capillary density, expression of the endothelial marker CD31 was determined. As depicted in Figure 4A, mRNA levels of CD31 were significantly reduced in quadriceps muscle in HFD-fed UniNx compared to sham-operated mice whereas no difference was observed in chow-fed mice (Supplementary Figure 3). Moreover, capillary-to-fiber ratio was significantly (~ 15%) reduced in skeletal muscle of HFD-fed UniNx mice (Figures 4B and 4C). Thus, uninephrectomy reduces muscle capillary density in HFD-fed mice. Mechanistically, reduced muscle capillary density may be the result of reduced HIF1α levels, which is a transcriptional activator of genes encoding vascular endothelial growth factor (VEGF) and other important mediators of angiogenesis (35). Indeed, HIF1α and VEGF-A mRNA levels were decreased in skeletal muscle of HFD-fed UniNx mice (Figure 4D). Moreover, protein levels of VEGF-A were decreased by 40% in skeletal muscle of HFD-fed UniNx compared to sham-operated mice (Figure 4E).

Improved hepatic insulin sensitivity in telmisartan-treated HFD-fed sham-operated mice

As reported in Table 2, angiotensin I levels were significantly increased in HFD-fed UniNx mice. Activation of the renin-angiotensin system (RAS) was previously suggested to contribute to HFD-associated skeletal muscle insulin resistance (36-38). Thus, we hypothesized that the observed increase in circulating angiotensin I concentration may deteriorate HFD-induced skeletal muscle insulin resistance via activation of angiotensin II type 1 receptors (AT1R). To test such hypothesis we made use of the AT1R blocker telmisartan. UniNx and sham-operated mice were fed a HFD for 20 weeks and received telmisartan in the drinking water at a dose of 3mg/kg*day during the entire period. As depicted in Figures 5A and 5B telmisartan treatment

improved glucose tolerance in HFD-fed sham-operated but not UniNx mice. Moreover, it improved glucose infusion rate (Figure 5C) and hepatic insulin sensitivity (Figure 5D) in sham-operated mice as analyzed by hyperinsulinemic-euglycemic clamp studies (see Supplementary Figure 4 for detailed time courses). In accordance with elevated hepatic insulin sensitivity, telmisartan treatment reduced hepatic steatosis in sham-operated mice (total liver lipids in untreated HFD-fed sham-operated mice: 299.4 ± 59.6 mg/g liver tissue; total liver lipids in telmisartan-treated HFD-fed sham-operated mice: 158.0 ± 31.8 mg/g liver tissue) but did not affect it in UniNx mice (total liver lipids in untreated HFD-fed UniNx mice: 123.4 ± 17.7 mg/g liver tissue; total liver lipids in telmisartan-treated HFD-fed UniNx mice: 178.5 ± 22.8 mg/g liver tissue) resulting in similar total liver lipids in telmisartan-treated mice of both groups (Figure 5E). Moreover, mRNA expression levels of pro-inflammatory cytokines in mesenteric adipose tissue were similar between telmisartan-treated HFD-fed sham-operated and UniNx mice (Figure 5F). Of note, expression of HIF1α was no longer different between telmisartan-treated sham-operated and UniNx mice (Figure 5F). Such data suggest that telmisartan treatment improved adipose tissue inflammation in HFD-fed sham-operated mice since the observed difference in cytokine mRNA expression in untreated mice (Figure 2A) was no longer present.

No effect of telmisartan treatment on muscle insulin resistance and capillary rarefaction in HFD-fed UniNx mice

Previously, the angiotensin II receptor blocker losartan was found to reverse insulin resistance through the modulation of muscular circulation in rats with impaired glucose metabolism (20). We therefore postulated that telmisartan would improve

muscle insulin sensitivity as well as capillary density in UniNx mice. However, as depicted in Figure 6A, 20 weeks of telmisartan treatment did not affect insulin-stimulated glucose disposal rate (IS-GDR) in UniNx mice (IS-GDR in untreated HFD-fed UniNx mice: 10.6 ± 1.2 mg/kg*min; IS-GDR in telmisartan-treated HFD-fed UniNx mice: 4.2 ± 2.3 mg/kg*min). Accordingly, insulin stimulated glucose uptake was significantly higher in telmisartan-treated HFD-fed sham-operated compared to UniNx mice (Figure 6B). Moreover, CD31 expression remained reduced in quadriceps muscle of telmisartan-treated HFD-fed UniNx compared to sham-operated mice (Figure 6C). Thus, telmisartan treatment positively impacts on total body and hepatic insulin sensitivity in HFD-fed sham-operated mice but does not affect impaired skeletal muscle insulin sensitivity in HFD-fed UniNx mice.

Discussion

In the present study we describe an unexpected dissociation of hepatic and muscle insulin resistance: whereas uninephrectomy protected HFD-fed mice from the development of hepatic insulin resistance (and hepatic steatosis), it deteriorated skeletal muscle insulin resistance.

The observed association of reduced visceral adipose tissue inflammation and improved hepatic insulin sensitivity in HFD-fed UniNx mice is in accordance with the “portal theory” claiming that the exaggerated release of FFAs and/or pro-inflammatory cytokines from visceral fat are directly delivered to the liver via portal vein, promoting the development of hepatic insulin resistance and hepatic steatosis (34). Interestingly, expression of HIF1α was reduced in adipose tissue of UniNx mice. Selective inhibition of

HIF1α was previously reported to reduce adipose tissue inflammation as well as hepatic steatosis in HFD-fed mice (39). Conversely, overexpression of HIF1α induced adipose tissue fibrosis and inflammation as well as hepatic steatosis (40). Thus, uninephrectomy is associated with decreased HIF1α expression in adipose tissue and thereby may contribute to reduced adipose tissue inflammation and, consequently, preserved hepatic insulin sensitivity. Such notion is further supported by the fact that treatment with telmisartan abolished differences in mRNA expression of HIF1α as well as pro-inflammatory cytokines and improved hepatic insulin sensitivity in sham-operated mice.

The kidney contributes to a significant part (~15-20%) to endogenous glucose production in both humans and rats (41; 42). Thus, basal endogenous glucose production may be reduced in UniNx mice. However, similar basal endogenous glucose production was observed in HFD-fed UniNx and sham-operated mice (UniNx: 25.8 mg/kg*min, sham-operated: 22.2 mg/kg*min; p=0.27). Moreover, insulin-mediated suppression of endogenous glucose production was increased in HFD-fed UniNx mice. Since renal glucose production is inhibited by insulin we cannot exclude that such improvement may be due to improved renal insulin sensitivity in UniNx mice. However, the fact that adipose tissue inflammation as well as liver lipid accumulation was decreased in HFD-fed UniNx mice and the notion that endogenous glucose production mainly reflects hepatic glucose production renders improved hepatic insulin sensitivity a more likely explanation herein.

Decreased mRNA expression and histological staining of CD31 point towards reduced capillary density in skeletal muscle of HFD-fed UniNx mice. Capillary rarefaction was previously associated with insulin resistance both in humans and rodents (19-21). In accordance with our findings presented herein, Flisinski et al reported reduced numbers of capillaries as well as a decreased capillary-to-fiber ratio in gastrocnemius and longissimus muscle in UniNx male Wistar rats (43). Such changes were already

present at an early stage and independent of blood pressure. Of note, treatment with the angiotensin II receptor blocker telmisartan had no impact on capillary density in UniNx mice suggesting that UniNx-associated capillary rarefaction is not dependent on activation of the RAS whereas it may modulate muscular circulation and thereby insulin sensitivity as was previously reported for the angiotensin II receptor blocker losartan in rats (20). Herein, reduced capillary density was associated with decreased HIF1α mRNA expression in skeletal muscle of UniNx mice. HIF1α is the master regulator of transcriptional responses to hypoxia and a transcriptional activator of genes encoding vascular endothelial growth factor (VEGF) and other important mediators of angiogenesis (35). Indeed, VEGF-A mRNA and protein levels were reduced in HFD-fed UniNx compared to sham-operated mice suggesting that reduced HIF1α may be responsible for reduced capillary density in the former. Importantly, UniNx and subtotal nephrectomy in Wistar rats were associated with reduced expression of HIF1α, VEGF A and VEGF receptor in gastrocnemius muscle (44). In addition, subtotal nephrectomy reduced skeletal muscle angiogenesis in rats (45). Unfortunately, HIF1α expression was not determined in the latter publication. Moreover, muscle-specific deletion of VEGF resulted in capillary rarefaction and diminished insulin-induced muscle glucose uptake *in vivo* independent of defects in insulin action at the myocyte (22). Thus, reduced expression of HIF1α may be causally linked to reduced capillary density observed in skeletal muscle of UniNx mice.

In conclusion, UniNx unexpectedly protects mice from HFD-induced adipose tissue inflammation and hepatic insulin resistance potentially via a reduction in HIF1α expression. In contrast, UniNx leads to capillary rarefaction in skeletal muscle and, thus, deteriorates HFD-induced skeletal muscle glucose disposal *in vivo*.

Acknowledgments

This work was supported by grants from the Swiss National Center for Competence in Research NCCR-Kidney.ch (to GAKU and DK), the Swiss National Science Foundation (#310030-141238) (to DK), the Foundation for Research at the Medical Faculty, University of Zurich (to FI) and the International Fellowship Program (grant no. 246539) on Integrative Kidney Physiology and Pathophysiology (IKPP; to GAKU). MSFW was supported by the Wolfermann-Nägeli-Stiftung. We would like to greatly acknowledge Prof. Giatgen Spinas, University Hospital Zurich, for continuous support, and Dr. Denis Arsenijevic as well as Prof. Jean-Pierre Montani, University of Fribourg, for expert advice regarding the uninephrectomy procedure. Telmisartan was kindly provided by Boehringer Ingelheim International GmbH (MTA 1037).

Author Contributions

DK conceived the study and wrote the paper. SHC, FI, SW, ZZ, MSFW and ZG performed the experimental work. EJS, GAKU and HAH gave conceptual advice. All authors contributed to discussion and reviewed/edited manuscript.

Conflict of interests' statement

All authors state no conflict of interest.

References

1. DeFronzo RA, Alvestrand A, Smith D, Hendler R, Hendler E, Wahren J: Insulin resistance in uremia. J Clin Invest 1981;67:563-568
2. Shehab-Eldin W, Zaki A, Gazareen S, Shoker A: Susceptibility to hyperglycemia in patients with chronic kidney disease. Am J Nephrol 2009;29:406-413
3. Ferreira-Filho SR, da Silva Passos L, Ribeiro MB: Corporeal weight gain and metabolic syndrome in living kidney donors after nephrectomy. Transplant Proc 2007;39:403-406
4. Shehab-Eldin W, Shoeb S, Khamis S, Salah Y, Shoker A: Susceptibility to insulin resistance after kidney donation: a pilot observational study. Am J Nephrol 2009;30:371-376
5. Sui Y, Zhao HL, Ma RC, Ho CS, Kong AP, Lai FM, Ng HK, Rowlands DK, Chan JC, Tong PC: Pancreatic islet beta-cell deficit and glucose intolerance in rats with uninephrectomy. Cell Mol Life Sci 2007;64:3119-3128
6. Zhao HL, Sui Y, Guan J, He L, Zhu X, Fan RR, Xu G, Kong AP, Ho CS, Lai FM, Rowlands DK, Chan JC, Tong PC: Fat redistribution and adipocyte transformation in uninephrectomized rats. Kidney Int 2008;74:467-477
7. Yvan-Charvet L, Quignard-Boulange A: Role of adipose tissue renin-angiotensin system in metabolic and inflammatory diseases associated with obesity. Kidney Int 2011;79:162-168
8. Kouyama R, Suganami T, Nishida J, Tanaka M, Toyoda T, Kiso M, Chiwata T, Miyamoto Y, Yoshimasa Y, Fukamizu A, Horiuchi M, Hirata Y, Ogawa Y: Attenuation of diet-induced weight gain and adiposity through increased energy expenditure in mice lacking angiotensin II type 1a receptor. Endocrinology 2005;146:3481-3489
9. Lee MH, Song HK, Ko GJ, Kang YS, Han SY, Han KH, Kim HK, Han JY, Cha DR: Angiotensin receptor blockers improve insulin resistance in type 2 diabetic rats by modulating adipose tissue. Kidney Int 2008;74:890-900
10. Chujo D, Yagi K, Asano A, Muramoto H, Sakai S, Ohnishi A, Shintaku-Kubota M, Mabuchi H, Yamagishi M, Kobayashi J: Telmisartan treatment decreases visceral fat accumulation and improves serum levels of adiponectin and vascular inflammation markers in Japanese hypertensive patients. Hypertens Res 2007;30:1205-1210
11. Foryst-Ludwig A, Hartge M, Clemenz M, Sprang C, Hess K, Marx N, Unger T, Kintscher U: PPARgamma activation attenuates T-lymphocyte-dependent inflammation of adipose tissue and development of insulin resistance in obese mice. Cardiovasc Diabetol 2010;9:64
12. Zhao ZQ, Luo R, Li LY, Tian FS, Zheng XL, Xiong HL, Sun LT: Angiotensin II Receptor Blocker Telmisartan Prevents New-Onset Diabetes in Pre-Diabetes OLETF Rats on a High-Fat Diet: Evidence of Anti-Diabetes Action. Can J Diabetes 2013;37:156-168
13. Rattigan S, Clark MG, Barrett EJ: Acute vasoconstriction-induced insulin resistance in rat muscle in vivo. Diabetes 1999;48:564-569
14. Solomon TP, Haus JM, Li Y, Kirwan JP: Progressive hyperglycemia across the glucose tolerance continuum in older obese adults is related to skeletal muscle capillarization and nitric oxide bioavailability. J Clin Endocrinol Metab 2011;96:1377-1384
15. Chiu JD, Richey JM, Harrison LN, Zuniga E, Kolka CM, Kirkman E, Ellmerer M, Bergman RN: Direct administration of insulin into skeletal muscle reveals that the

transport of insulin across the capillary endothelium limits the time course of insulin to activate glucose disposal. Diabetes 2008;57:828-835
16. Ellmerer M, Hamilton-Wessler M, Kim SP, Huecking K, Kirkman E, Chiu J, Richey J, Bergman RN: Reduced access to insulin-sensitive tissues in dogs with obesity secondary to increased fat intake. Diabetes 2006;55:1769-1775
17. Fueger PT, Shearer J, Bracy DP, Posey KA, Pencek RR, McGuinness OP, Wasserman DH: Control of muscle glucose uptake: test of the rate-limiting step paradigm in conscious, unrestrained mice. J Physiol 2005;562:925-935
18. Halseth AE, Bracy DP, Wasserman DH: Limitations to basal and insulin-stimulated skeletal muscle glucose uptake in the high-fat-fed rat. AmJ Physiol Endocrinol Metab 2000;279:E1064-1071
19. Gavin TP, Stallings HW, 3rd, Zwetsloot KA, Westerkamp LM, Ryan NA, Moore RA, Pofahl WE, Hickner RC: Lower capillary density but no difference in VEGF expression in obese vs. lean young skeletal muscle in humans. J Appl Physiol 2005;98:315-321
20. Guo Q, Mori T, Jiang Y, Hu C, Ohsaki Y, Yoneki Y, Nakamichi T, Ogawa S, Sato H, Ito S: Losartan modulates muscular capillary density and reverses thiazide diuretic-exacerbated insulin resistance in fructose-fed rats. Hypertens Res 2012;35:48-54
21. Marin P, Andersson B, Krotkiewski M, Bjorntorp P: Muscle fiber composition and capillary density in women and men with NIDDM. Diabetes Care 1994;17:382-386
22. Bonner JS, Lantier L, Hasenour CM, James FD, Bracy DP, Wasserman DH: Muscle-specific vascular endothelial growth factor deletion induces muscle capillary rarefaction creating muscle insulin resistance. Diabetes 2013;62:572-580
23. Konrad D, Rudich A, Schoenle EJ: Improved glucose tolerance in mice receiving intraperitoneal transplantation of normal fat tissue. Diabetologia 2007;50:833-839
24. Rytka JM, Wueest S, Schoenle EJ, Konrad D: The portal theory supported by venous drainage-selective fat transplantation. Diabetes 2011;60:56-63
25. Fisher SJ, Kahn CR: Insulin signaling is required for insulin's direct and indirect action on hepatic glucose production. J Clin Invest 2003;111:463-468
26. Kim JK, Michael MD, Previs SF, Peroni OD, Mauvais-Jarvis F, Neschen S, Kahn BB, Kahn CR, Shulman GI: Redistribution of substrates to adipose tissue promotes obesity in mice with selective insulin resistance in muscle. J Clin Invest 2000;105:1791-1797
27. Saberi M, Bjelica D, Schenk S, Imamura T, Bandyopadhyay G, Li P, Vargeese C, Wang W, Bowman K, Zhang Y, Polisky B, Olefsky JM: Novel liver-specific TORC2 siRNA corrects hyperglycemia in rodent models of type 2 diabetes. Am J Physiol Endocrinol Metab 2009;297:E1137-E1146
28. Bruce CR, Risis S, Babb JR, Yang C, Kowalski GM, Selathurai A, Lee-Young RS, Weir JM, Yoshioka K, Takuwa Y, Meikle PJ, Pitson SM, Febbraio MA: Overexpression of sphingosine kinase 1 prevents ceramide accumulation and ameliorates muscle insulin resistance in high-fat diet-fed mice. Diabetes 2012;61:3148-3155
29. Wueest S, Mueller R, Bluher M, Item F, Chin AS, Wiedemann MS, Takizawa H, Kovtonyuk L, Chervonsky AV, Schoenle EJ, Manz MG, Konrad D: Fas (CD95) expression in myeloid cells promotes obesity-induced muscle insulin resistance. EMBO Mol Med 2014;6:43-56

30. Hansen PA, Gulve EA, Holloszy JO: Suitability of 2-deoxyglucose for in vitro measurement of glucose transport activity in skeletal muscle. J Appl Physiol 1994;76:979-985
31. Knight JA, Anderson S, Rawle JM: Chemical basis of the sulfo-phospho-vanillin reaction for estimating total serum lipids. Clin Chem 1972;18:199-202
32. Bligh EG, Dyer WJ: A rapid method of total lipid extraction and purification. Can J Biochem Physiol 1959;37:911-917
33. Wueest S, Rapold RA, Schumann DM, Rytka JM, Schildknecht A, Nov O, Chervonsky AV, Rudich A, Schoenle EJ, Donath MY, Konrad D: Deletion of Fas in adipocytes relieves adipose tissue inflammation and hepatic manifestations of obesity in mice. J Clin Invest 2010;120:191-202
34. Item F, Konrad D: Visceral fat and metabolic inflammation: the portal theory revisited. Obes Rev 2012;13 Suppl 2:30-39
35. Semenza GL: Angiogenesis in ischemic and neoplastic disorders. Annu Rev Med 2003;54:17-28
36. Diamond-Stanic MK, Henriksen EJ: Direct inhibition by angiotensin II of insulin-dependent glucose transport activity in mammalian skeletal muscle involves a ROS-dependent mechanism. Arch Physiol Biochem 2010;116:88-95
37. Henriksen EJ, Prasannarong M: The role of the renin-angiotensin system in the development of insulin resistance in skeletal muscle. Mol Cell Endocrinol 2012;378:15-22
38. Wei Y, Sowers JR, Clark SE, Li W, Ferrario CM, Stump CS: Angiotensin II-induced skeletal muscle insulin resistance mediated by NF-kappaB activation via NADPH oxidase. Am J Physiol Endocrinol Metab 2008;294:E345-351
39. Sun K, Halberg N, Khan M, Magalang UJ, Scherer PE: Selective inhibition of hypoxia-inducible factor 1alpha ameliorates adipose tissue dysfunction. Mol Cell Biol 2013;33:904-917
40. Halberg N, Khan T, Trujillo ME, Wernstedt-Asterholm I, Attie AD, Sherwani S, Wang ZV, Landskroner-Eiger S, Dineen S, Magalang UJ, Brekken RA, Scherer PE: Hypoxia-inducible factor 1alpha induces fibrosis and insulin resistance in white adipose tissue. Mol Cell Biol 2009;29:4467-4483
41. Gerich JE, Meyer C, Woerle HJ, Stumvoll M: Renal gluconeogenesis: its importance in human glucose homeostasis. Diabetes Care 2001;24:382-391
42. Pillot B, Soty M, Gautier-Stein A, Zitoun C, Mithieux G: Protein feeding promotes redistribution of endogenous glucose production to the kidney and potentiates its suppression by insulin. Endocrinology 2009;150:616-624
43. Flisinski M, Brymora A, Elminowska-Wenda G, Bogucka J, Walasik K, Stefanska A, Odrowaz-Sypniewska G, Manitius J: Influence of different stages of experimental chronic kidney disease on rats locomotor and postural skeletal muscles microcirculation. Ren Fail 2008;30:443-451
44. Flisinski M, Brymora A, Bartlomiejczyk I, Wisniewska E, Golda R, Stefanska A, Paczek L, Manitius J: Decreased hypoxia-inducible factor-1alpha in gastrocnemius muscle in rats with chronic kidney disease. Kidney Blood Press Res 2012;35:608-618
45. Jacobi J, Porst M, Cordasic N, Namer B, Schmieder RE, Eckardt KU, Hilgers KF: Subtotal nephrectomy impairs ischemia-induced angiogenesis and hindlimb re-perfusion in rats. Kidney Int 2006;69:2013-2021

Figure Legends

Figure 1 Improved hepatic but deteriorated muscle insulin sensitivity in HFD-fed UniNx mice

Intra-peritoneal glucose (**A**) and insulin tolerance (**B**) tests in chow-fed and HFD-fed sham-operated and UniNx mice are shown. Black squares: chow sham-operated (n=7); grey squares: chow UniNx (n=6); black circles: HFD sham-operated (n=15-17); grey circles: HFD UniNx (n=14-17). (**C** to **E**) Glucose infusion rate, inhibition of endogenous glucose production and insulin-stimulated glucose disposal rate (IS GDR) during hyperinsulinemic-euglycemic clamps in HFD-fed mice (n=5). Error bars represent SEM. *$p < 0.05$ and **$p < 0.01$ (Student's *t*-test).

Figure 2 Reduced hepatic steatosis and adipose tissue inflammation in HFD-fed UniNx mice

(**A**) Total liver lipids were determined and expressed relative to total liver weight in HFD-fed sham-operated (black bars) and UniNx mice (grey bars). (**B**) Representative hematoxylin- and eosin-stained histological sections of liver of HFD-fed sham-operated and UniNx mice. Scale bar represents 50 μm. (**C**) mRNA expression of respective genes in mesenteric adipose tissue of HFD-fed sham-operated (black bars) and UniNx mice (grey bars). n=5-10. *$p < 0.05$ (Student's *t*-test). (**D**) Representative hematoxylin- and eosin-stained histological sections of epididymal adipose tissue of HFD-fed sham-operated and UniNx mice. Scale bar represents 100 μm. (**E**) Adipocyte cell perimeter was measured using ImageJ. Up to 100 cells per fat pad of four different mice per group were analyzed. (**F**) Lysates of white adipose tissue were prepared, resolved by LDS-

PAGE and immunoblotted with anti-pS473 Akt, anti-total Akt or anti-actin antibody. Graphs show results of 4-5 mice. *p < 0.05 (Student's *t*-test). All error bars represent SEM.

Figure 3 Preserved/sustained insulin-stimulated glucose uptake into skeletal muscle *ex vivo*

Glucose uptake into intact isolated soleus muscle (**A**) and extensor digitorum longus (EDL) muscle (**B**) was measured in the absence (open bars) or presence of 120 nM insulin (filled bars). n=8. (**C**) Total muscle lysates were prepared, resolved by LDS-PAGE and immunoblotted with anti-pS473 Akt, anti-total Akt or anti-actin antibody. Graphs show results of 4-5 mice. Error bars represent SEM.

Figure 4 Reduced capillary density in skeletal muscle of HFD-fed UniNx mice

(**A**) mRNA expression of CD31 in quadriceps muscle of HFD-fed sham-operated (black bars) and UniNx mice (grey bars). n=4-5. (**B** and **C**) CD31 staining of quadriceps muscle harvested from HFD-fed sham-operated and UniNx mice. Capillary-to-fiber ratio was calculated after counting up to 700 fibers and corresponding capillaries per mouse. Scale bar represents 100 μm. n=4. (**D**) mRNA expression of HIF1α and VEGF-A in quadriceps muscle of HFD-fed sham-operated (black bars) and UniNx mice (grey bars). n=4-5. (**E**) Total muscle lysates were prepared, resolved by LDS-PAGE and immunoblotted with anti-VEGF-A or anti-actin antibody. Graphs show results of 8 mice. Error bars represent SEM. § p = 0.07, $^{\#}$ p = 0.06, *p < 0.05 (Student's *t*-test).

Figure 5 Improved hepatic insulin sensitivity in telmisartan-treated HFD-fed sham-operated mice

(**A**) Intra-peritoneal glucose-tolerance test in telmisartan-treated HFD-fed sham-operated (black circles) and UniNx (grey circles) mice. n=9-11. (**B**) Analysis of the area under the curve of glucose tolerance tests presented in A. (**C**) Glucose infusion rate and (**D**) inhibition of endogenous glucose production during hyperinsulinemic-euglycemic clamps. n=4. (**E**) Total liver lipids were determined and expressed relative to total liver weight in telmisartan-treated HFD-fed sham-operated (black bars) and UniNx mice (grey bars). n=5-6. All error bars represent SEM. (**F**) mRNA expression of respective genes in mesenteric adipose tissue of telmisartan-treated HFD-fed sham-operated (black bars) and UniNx mice (grey bars). n=4-5.Error bars represent SEM. *$p < 0.05$ and **$p < 0.01$ (Student's *t*-test).

Figure 6 No effect of telmisartan treatment on muscle insulin resistance and capillary rarefaction in HFD-fed UniNx mice

(**A**) Insulin-stimulated glucose disposal rate (IS GDR) and (**B**) insulin-stimulated glucose uptake into quadriceps muscle during hyperinsulinemic-euglycemic clamps. n=4. (**C**) mRNA expression of CD31 and HIF1α in quadriceps muscle of HFD-fed telmisartan-treated sham-operated (black bars) and UniNx mice (grey bars). n=4-5. *$p < 0.05$ and **$p < 0.01$ (Student's *t*-test).

Table 1 Body and organ weight in sham-operated and UniNx mice

	Sham-operated		UniNx	
	Chow	HFD	Chow	HFD
Body weight (g)				
- before surgery	24.5 ± 1.0	25.1 ± 0.6	24.4 ± 0.6	25.1 ± 0.8
- 20 weeks after	35.2 ± 0.7	51.2 ± 1.0	33.3 ± 0.7	50.4 ± 1.0
N	*7*	*22*	*8*	*22*
Kidney weight (mg)				
- right kidney	212 ± 6	231 ± 6	269 ± 7***	284 ± 11***
- left kidney	203 ± 5	209 ± 6	-	-
N	*7*	*8*	*8*	*7*
Liver weight (mg)	1576 ± 11.7	2458 ± 192##	1454 ± 45	2169 ± 145##
N	*7*	*13*	*8*	*12*
Fat pad weight (mg)				
- inguinal	576 ± 74	2479 ± 140###	428 ± 75	2362 ± 97###
- epididymal	899 ± 97	1857 ± 103###	887 ± 156	2382 ± 150**,###
- mesenteric	719 ± 158	1416 ± 89###	523 ± 59	1389 ± 131###
N	*7*	*13*	*8*	*12*

*p<0.05, **p<0.01, ***p<0.001 compared to sham-operated mice; #p<0.05, ##p<0.01, ###p<0.001 compared to chow-fed mice.

Table 2 Circulating blood levels in sham-operated and UniNx mice

	Sham-operated		UniNx	
	Chow	HFD	Chow	HFD
Glucose (mmol/l)	7.8 ± 0.7	11.7 ± 0.8$^{\#\#}$	8.8 ± 0.4	11.9 ± 0.8$^{\#\#}$
N	*7*	*10*	*8*	*10*
Insulin (ng/ml)	1.6 ± 0.2	7.0 ± 0.6$^{\#\#\#}$	0.9 ± 0.1**	5.9 ± 0.8$^{\#\#\#}$
N	*7*	*10*	*8*	*10*
FFA (mmol/l)	n.d.	0.72 ± 0.9	n.d.	0.79 ± 0.9
N		*5*		*5*
Creatinine (mg/dl)	n.d.	0.59 ± 0.03	n.d.	0.72 ± 0.03*
N		*7*		*9*
Uric acid (mg/dl)	n.d.	4.4 ± 0.4	n.d.	5.4 ± 0.8
N		*8*		*9*
Angiotensin I (ng/ml)	20.9 ± 2.0	20.6 ± 1.5	29.4 ± 1.8**	26.5 ± 1.5*
N	*6*	*8*	*6*	*9*
Bile acids (µmol/l)	8.4 ± 3.1	9.4 ± 1.3	8.2 ± 2.3	14.0 ± 4.0
N	*7*	*10*	*8*	*10*

*p<0.05, **p<0.01, ***p<0.001 compared to sham-operated mice; #p<0.05, ##p<0.01, ###p<0.001 compared to chow-fed mice.

Figure 1

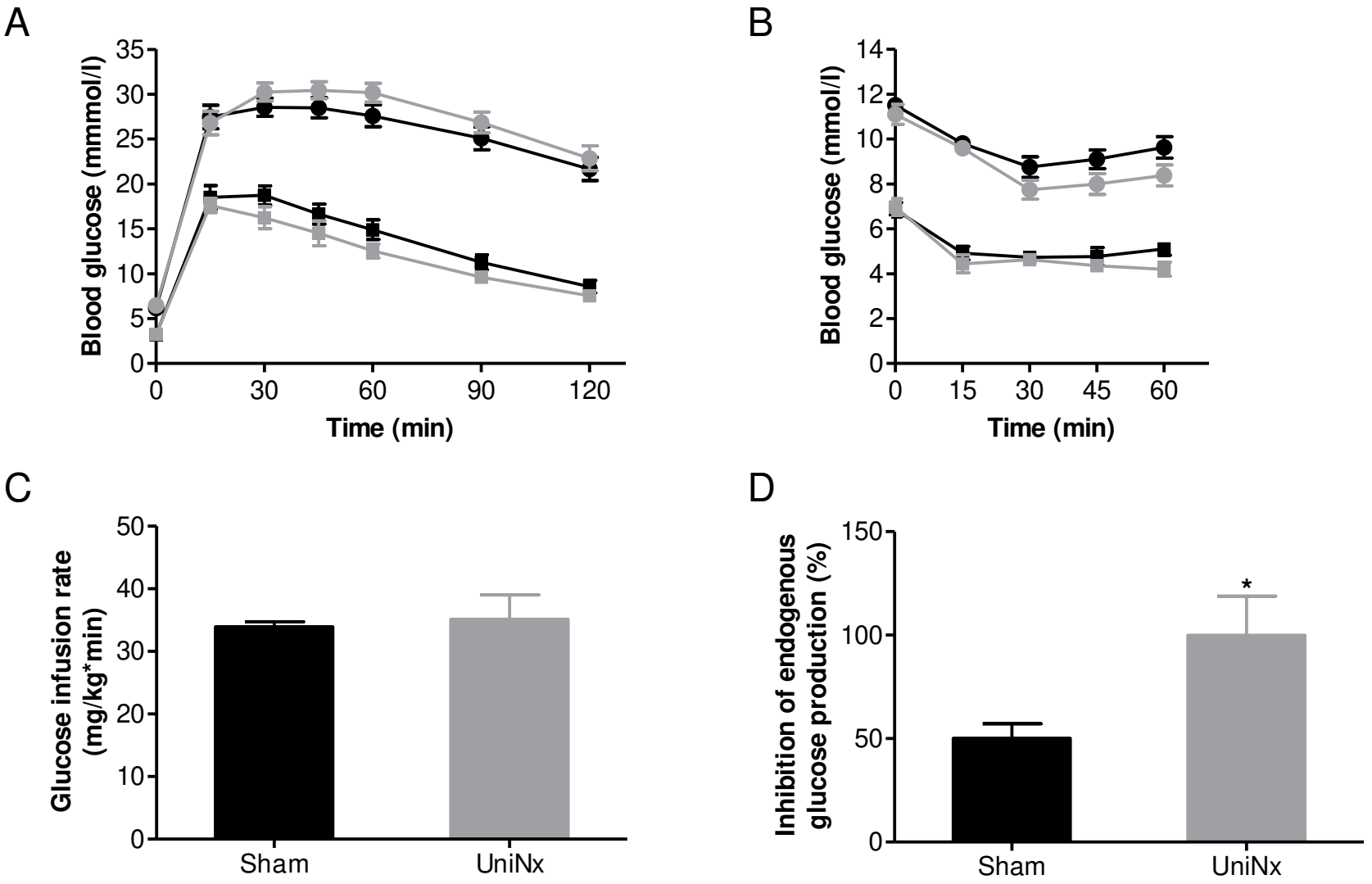
A
Blood glucose (mmmol/l)
35
30
25
20
15
10
5
0
0
30
60
90
120
Time (min)
B
Blood glucose (mmol/l)
14
12
10
8
6
4
2
0
0
15
30
45
60
Time (min)
C
Glucose infusion rate (mg/kg*min)
50
40
30
20
10
0
Sham
UniNx
D
Inhibition of endogenous glucose production (%)
150
100
50
0
*
Sham
UniNx

Figure 1

E

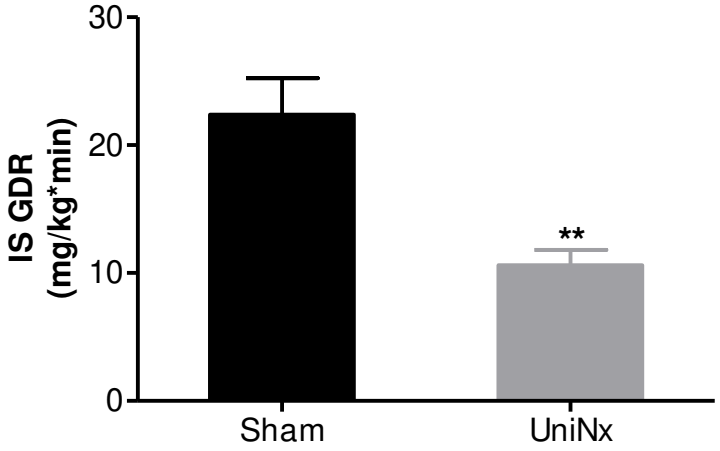

Figure 2

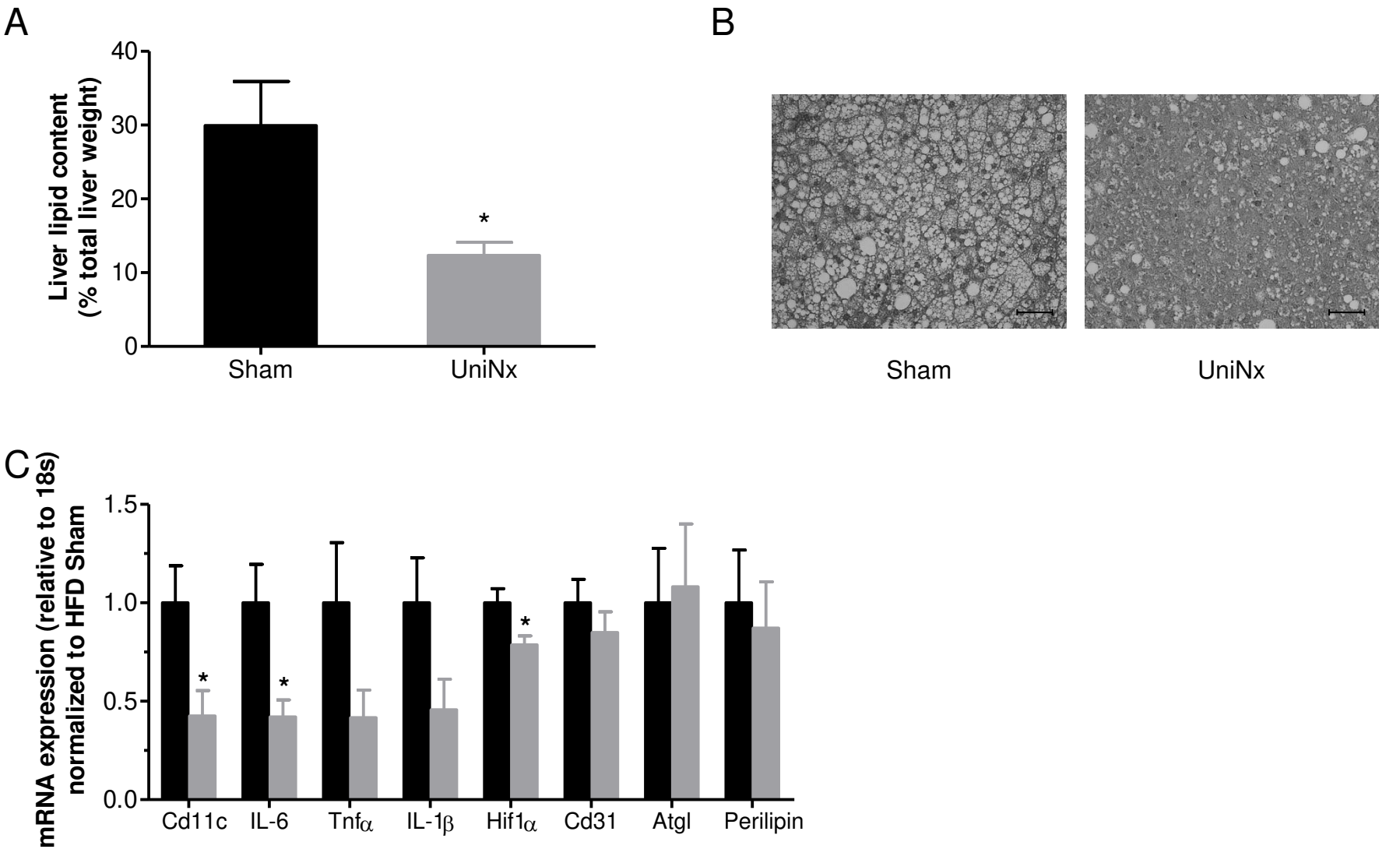
A
Liver lipid content (% total liver weight)
40
30
20
10
0
*
Sham
UniNx
B
Sham
UniNx
C
mRNA expression (relative to 18s) normalized to HFD Sham
1.5
1.0
0.5
0.0
*
*
*
Cd11c
IL-6
Tnfα
IL-1β
Hif1α
Cd31
Atgl
Perilipin

D

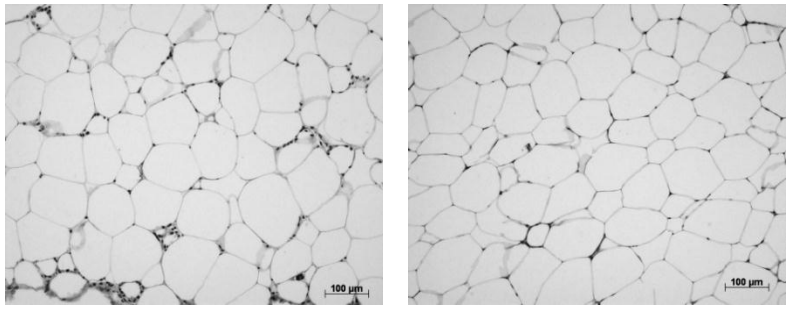
100 µm
100 µm
Sham
UniNx

E

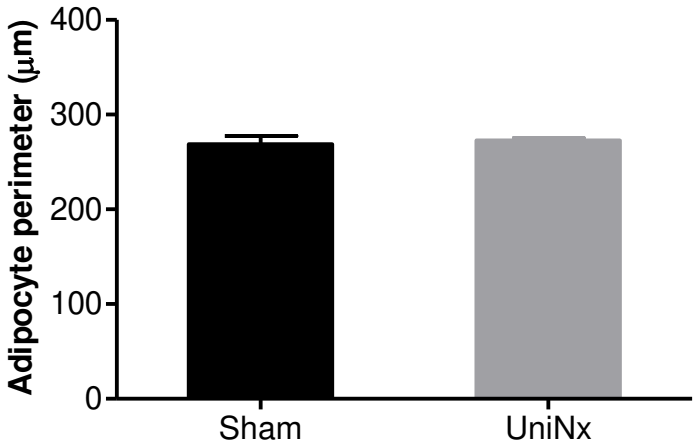
Adipocyte perimeter (µm)
400
300
200
100
0
Sham
UniNx

F

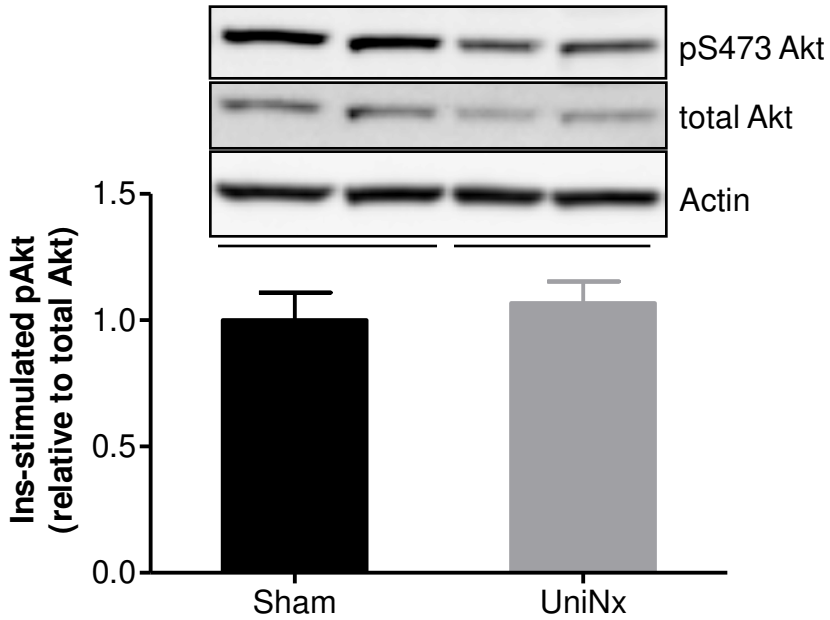
pS473 Akt
total Akt
Actin
Ins-stimulated pAkt
(relative to total Akt)
1.5
1.0
0.5
0.0
Sham
UniNx

Figure 3

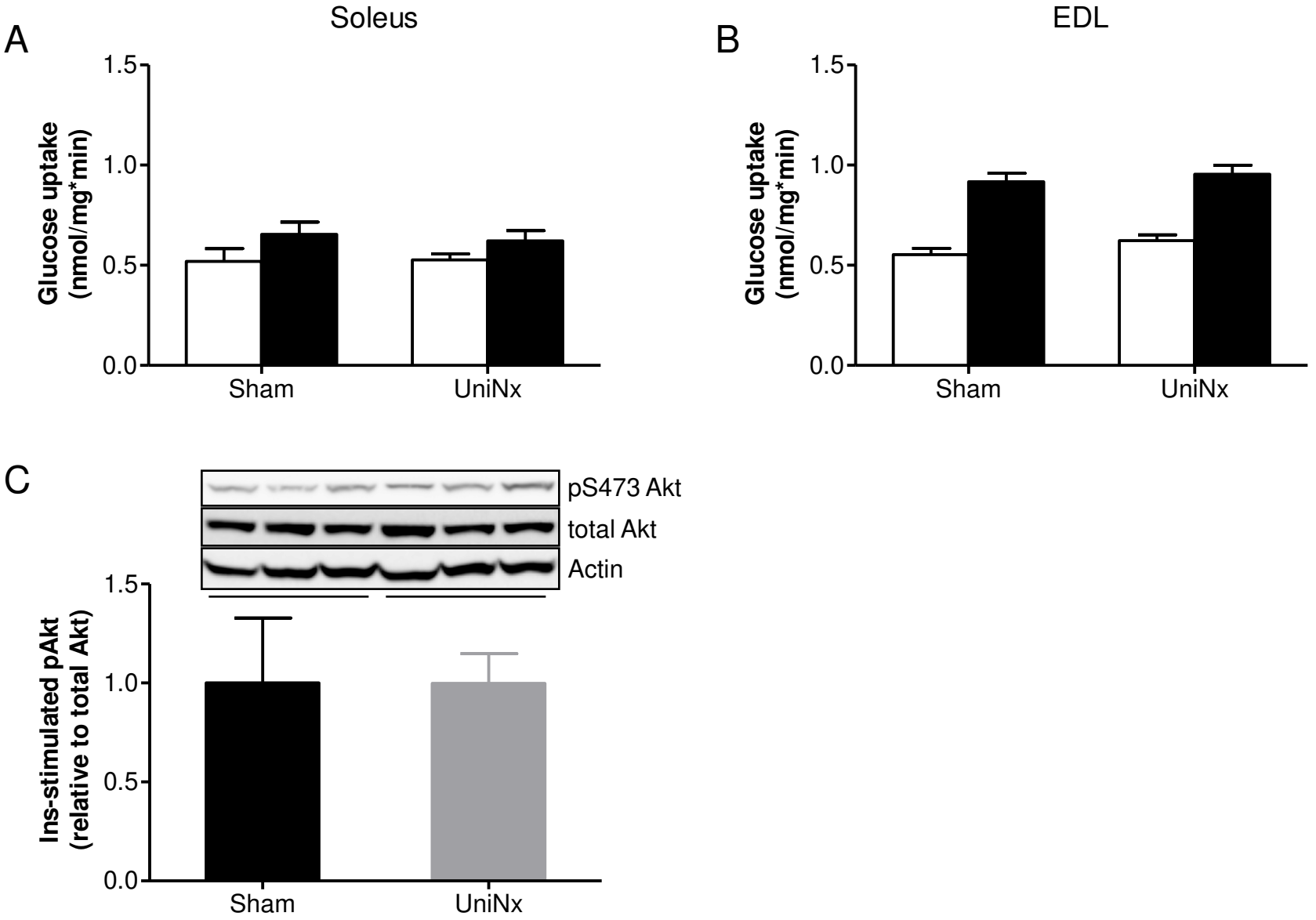
A
Soleus
Glucose uptake (nmol/mg*min)
1.5
1.0
0.5
0.0
Sham
UniNx
B
EDL
Glucose uptake (nmol/mg*min)
1.5
1.0
0.5
0.0
Sham
UniNx
C
pS473 Akt
total Akt
Actin
Ins-stimulated pAkt (relative to total Akt)
1.5
1.0
0.5
0.0
Sham
UniNx

Figure 4

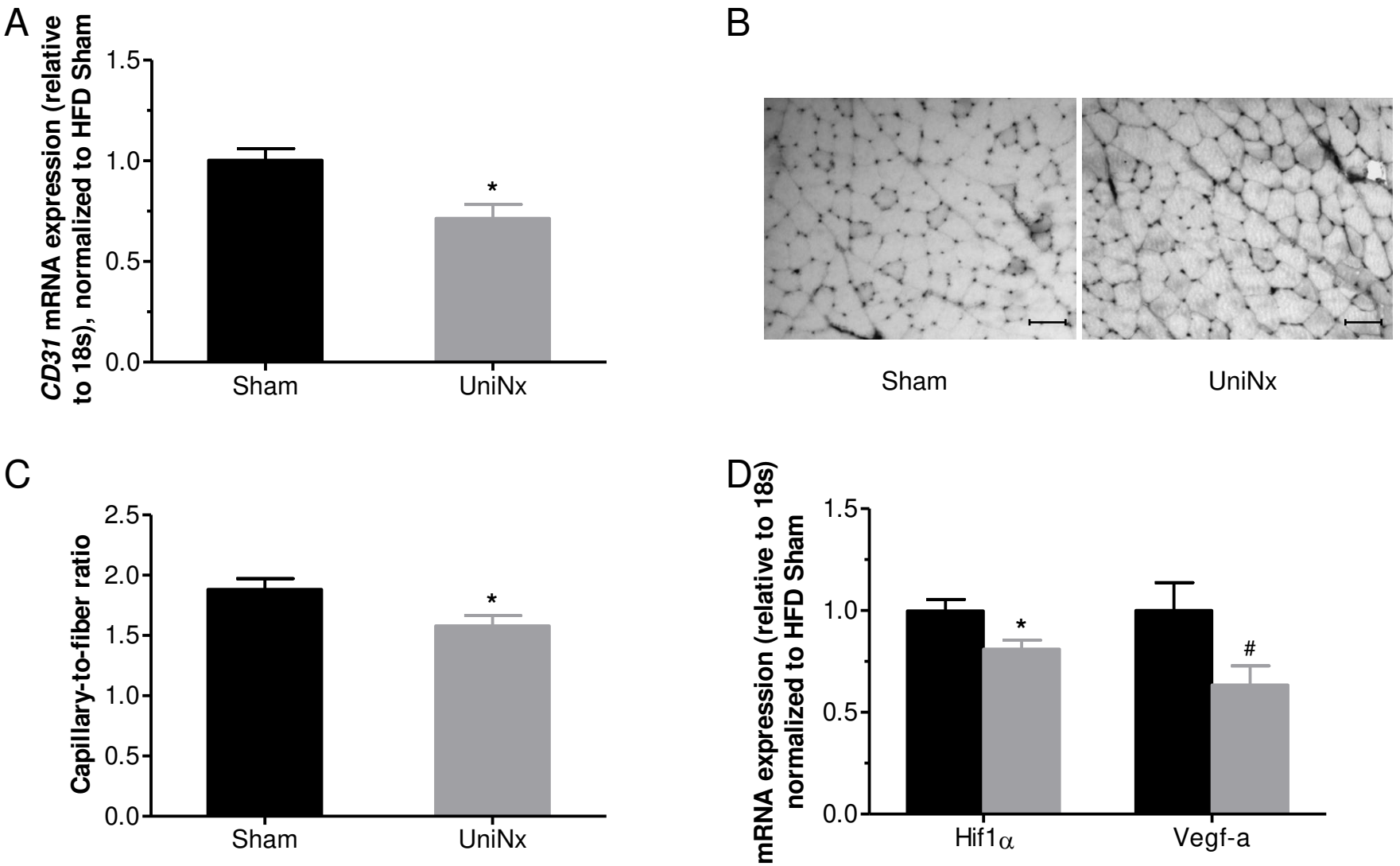
A
CD31 mRNA expression (relative to 18s), normalized to HFD Sham
1.5
1.0
0.5
0.0
*
Sham
UniNx
B
Sham
UniNx
C
Capillary-to-fiber ratio
2.5
2.0
1.5
1.0
0.5
0.0
*
Sham
UniNx
D
mRNA expression (relative to 18s) normalized to HFD Sham
1.5
1.0
0.5
0.0
*
#
Hif1α
Vegf-a

E

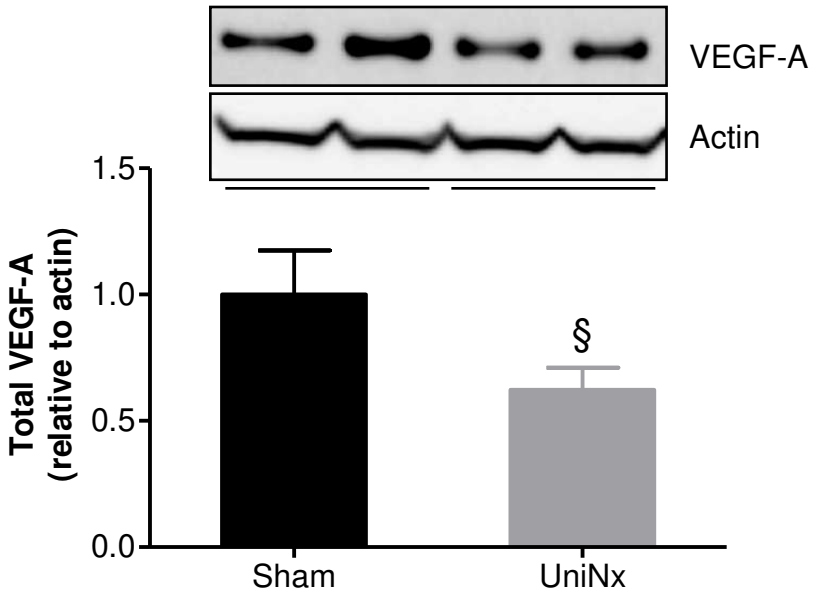
VEGF-A
Actin
1.5
1.0
0.5
0.0
Total VEGF-A
(relative to actin)
§
Sham
UniNx

Figure 5

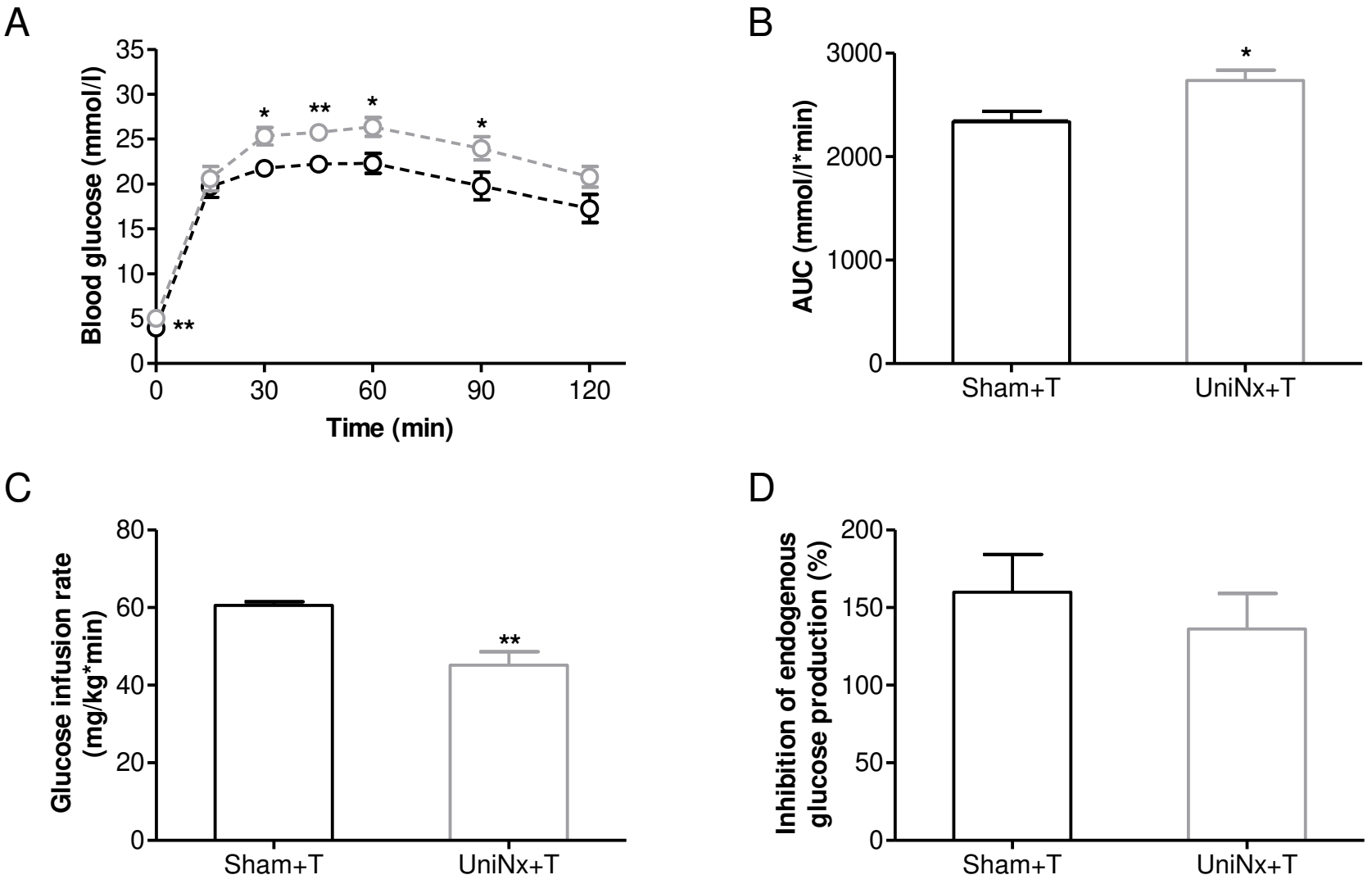
A
Blood glucose (mmol/l)
35
30
25
20
15
10
5
0
0
30
60
90
120
Time (min)
*
**
*
*
**
B
AUC (mmol/l*min)
3000
2000
1000
0
*
Sham+T
UniNx+T
C
Glucose infusion rate (mg/kg*min)
80
60
40
20
0
**
Sham+T
UniNx+T
D
Inhibition of endogenous glucose production (%)
200
150
100
50
0
Sham+T
UniNx+T

E

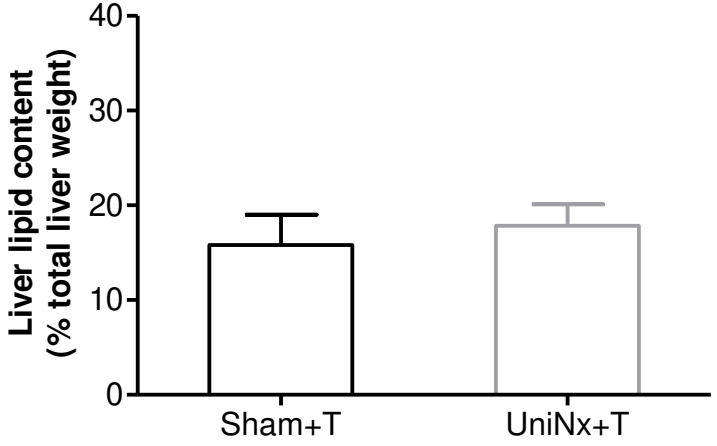
Liver lipid content
(% total liver weight)
40
30
20
10
0
Sham+T
UniNx+T

F

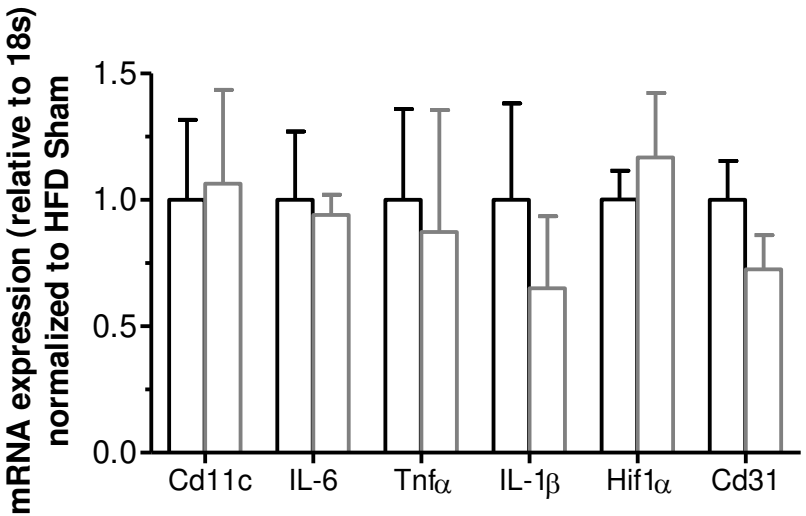
mRNA expression (relative to 18s)
normalized to HFD Sham
1.5
1.0
0.5
0.0
Cd11c
IL-6
Tnfα
IL-1β
Hif1α
Cd31

Figure 6

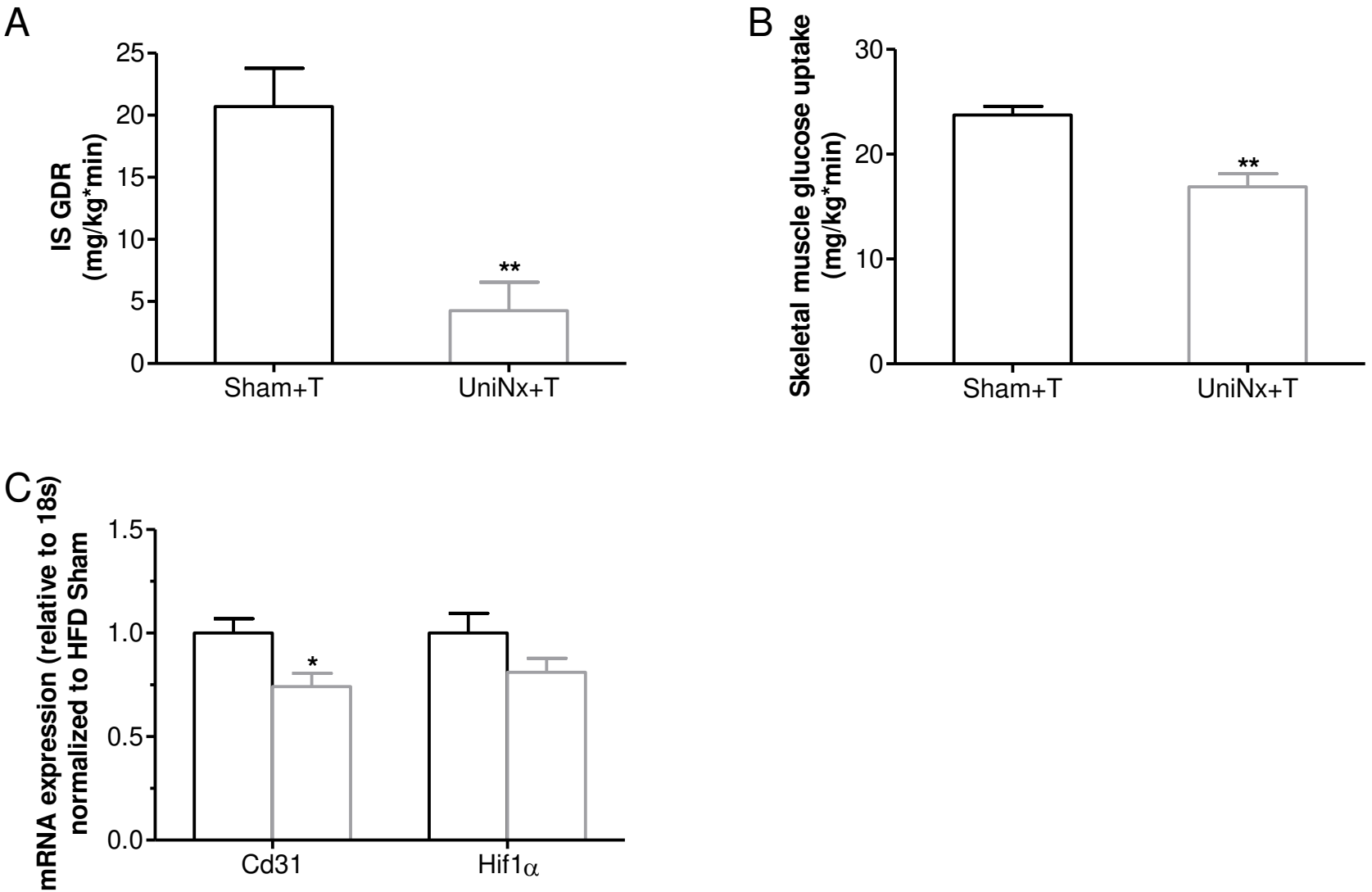
A
IS GDR (mg/kg*min)
25
20
15
10
5
0
**
Sham+T
UniNx+T
B
Skeletal muscle glucose uptake (mg/kg*min)
30
20
10
0
**
Sham+T
UniNx+T
C
mRNA expression (relative to 18s) normalized to HFD Sham
1.5
1.0
0.5
0.0
*
Cd31
Hif1α

Supplementary Figure 1

Similar respiratory quotient, locomotor activity and food intake in HFD-fed sham-operated and UniNx mice

(**A** and **B**) Respiratory quotient (RQ) and activity was determined in metabolic cages in HFD-fed sham-operated (black symbols) and UniNx (grey symbols) mice. (**C**) Food intake was measured in metabolic cages in HFD-fed sham-operated (black bars) and UniNx (grey bars) mice. n=7-8. Error bars represent SEM.

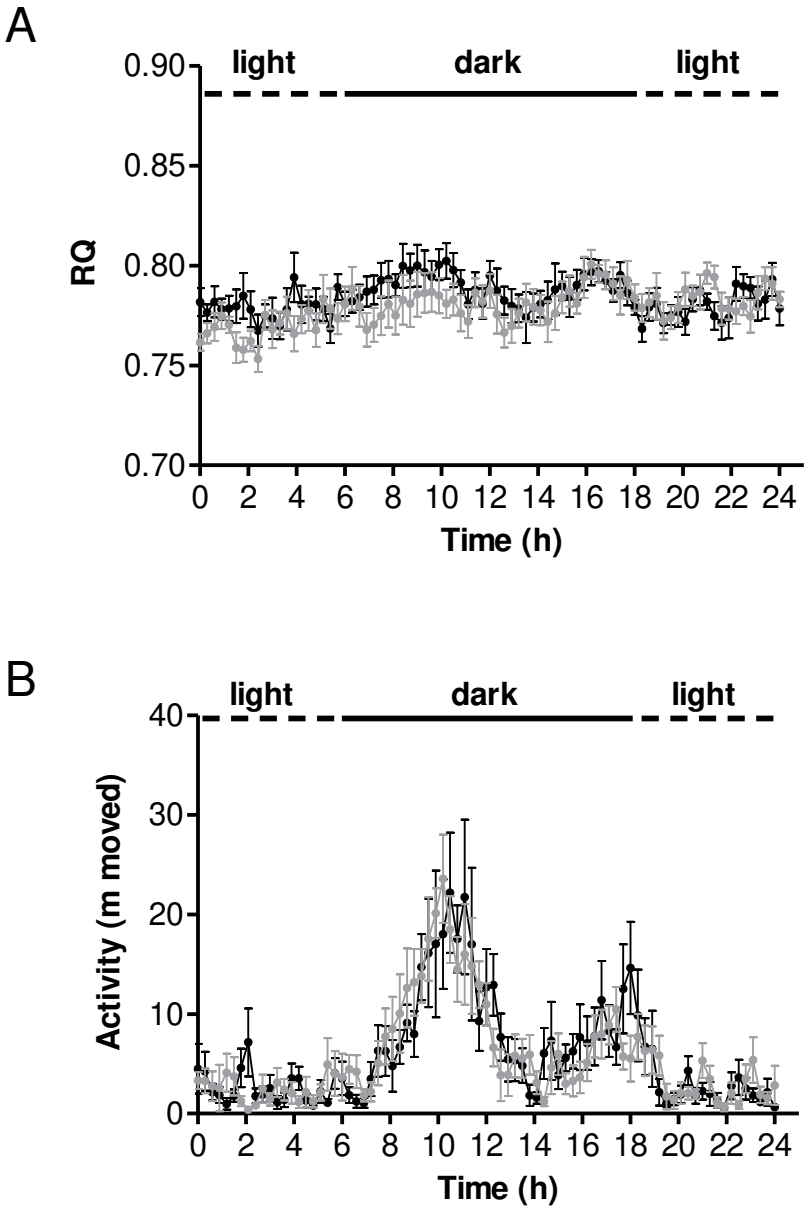

C

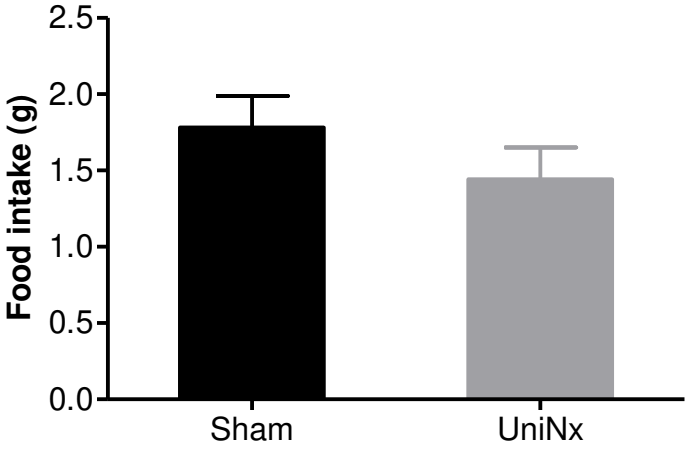

Supplementary Figure 2

Blood glucose concentrations and glucose infusion rates during hyperinsulinemic-euglycemic clamp

(**A**) Blood glucose levels were clamped upon insulin infusion at about 5 mmol/l in HFD-fed sham (black symbols) and UniNx (grey symbols) mice. n=5. (**B**) In order to maintain euglycemia, glucose infusion rate was adjusted over time. n=5.

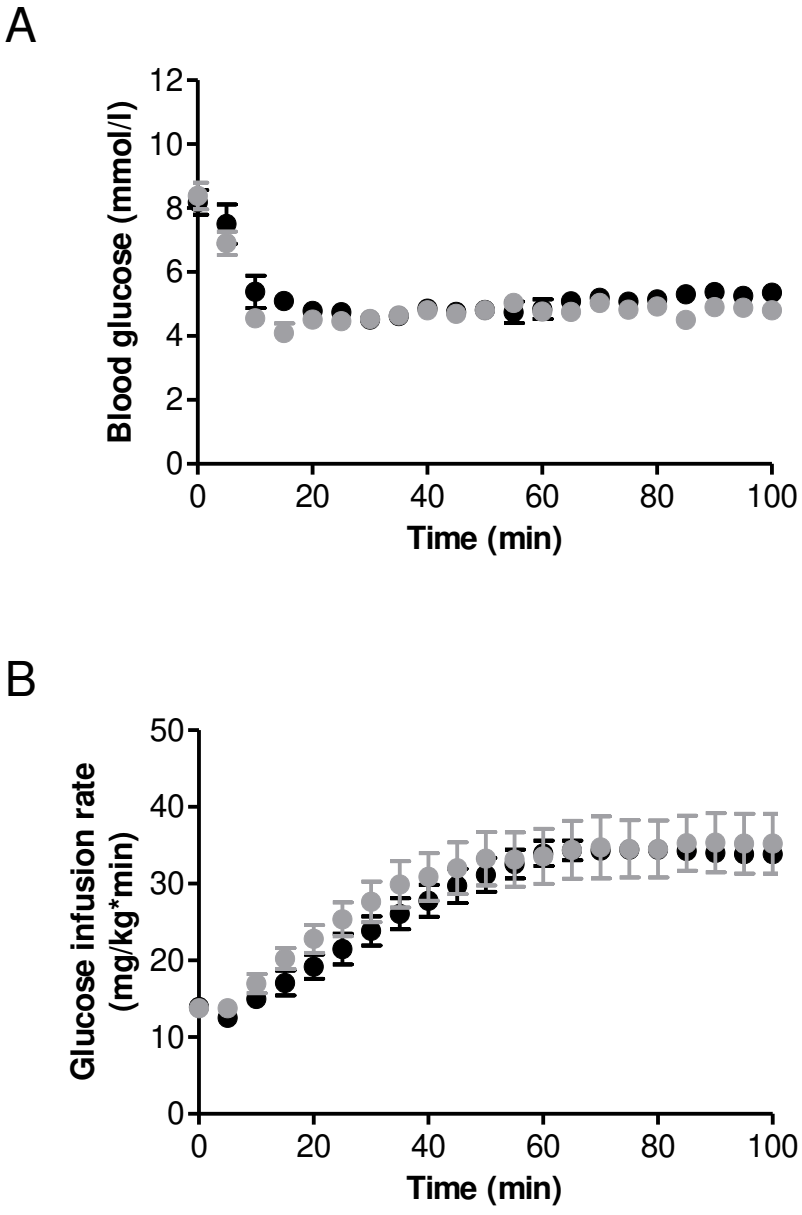

Supplementary Figure 3

Similar CD31 and HIF1α mRNA expression in chow-fed sham-operated and UniNx mice

mRNA expression of CD31 and HIF1α in quadriceps muscle of chow-fed sham-operated (black bars) and UniNx mice (grey bars). n=5.

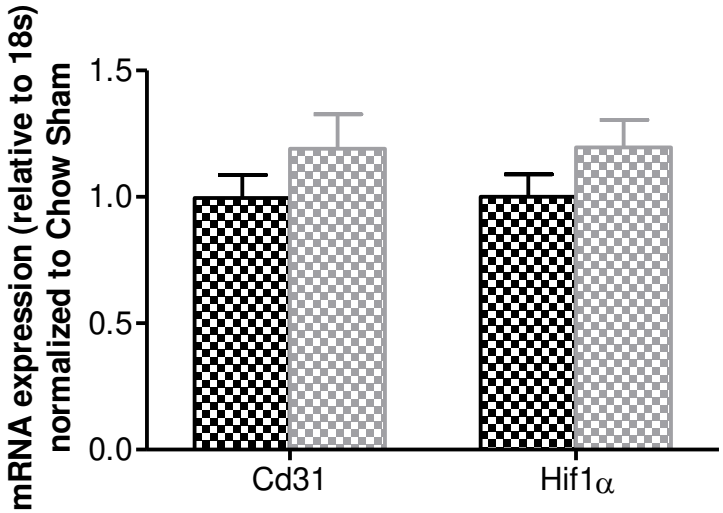

Supplementary Figure 4

Blood glucose concentrations and glucose infusion rates during hyperinsulinemic-euglycemic clamp in telmisartan-treated HFD-fed mice
(**A**) Blood glucose levels were clamped upon insulin infusion at about 5 mmol/l in telmisartan-treated HFD-fed sham (black circles) and UniNx (grey circles) mice. n=5.
(**B**) In order to maintain euglycemia, glucose infusion rate was adjusted over time. n=5.